JOURNAL OF AGRICULTURAL AND FOOD CHEMISTRY

Article

pubs.acs.org/JAFC

Synthesis and Insecticidal Activity of Enzyme-Triggered Functionalized Hollow Mesoporous Silica for Controlled Release

Amir E. Kaziem,[†,‡] Yunhao Gao,[†] Shun He,*[,†] and Jianhong Li*[,†]

[†]Hubei Insect Resources Utilization and Sustainable Pest Management Key Laboratory, College of Plant Science and Technology, Huazhong Agricultural University, Wuhan 430070, China

[‡]Department of Environmental Agricultural Science, Institute of Environmental Studies and Research, Ain Shams University, Cairo 11566, Egypt

Supporting Information

ABSTRACT: In the present study, enzymatic responsive controlled release formulations (CRFs) were fabricated. The CRFs were achieved by anchoring mechanically interlocked molecules using α-cyclodextrin onto the surface pore rims of hollow mesoporous silica (HMS). The CRFs were characterized using Fourier transform infrared spectroscopy, scanning electron microscopy, transmission electron microscopy, and thermogravimetric analysis. The results showed that the CRFs had extraordinary loading ability for chlorantraniliprole (42% w/w) and could effectively preserve chlorantraniliprole against degradation under thermal conditions and UV radiation. The CRFs have been proven to be enzyme-sensitive. The release ratio of chlorantraniliprole from CRFs can be accelerated observably when external α-amylase was introduced. The persistence of CRFs was evaluated by regular sampling feeding experiment using *Plutella xylostella* as the target insect. The results showed that the larval mortality of *P. xylostella* was much higher than that of Coragen under all concentrations after 14 days, which proved that CRFs had remarkable persistence.

KEYWORDS: *chlorantraniliprole, hollow mesoporous silica, controlled release, α-amylase sensitivity, biological activity survey*

INTRODUCTION

Chewing insects are considered the most injurious enemy for crops, not only for their feeding consequences on shoots and roots but also leaving plants vulnerable to infections with virus, fungi, and bacteria.[1] Over the last several decades, pesticide preparation has focused on extending the active ingredient validity period in the ecosystem as much as possible[2] but did not consider the environmental exposure period.[3] This dilemma can be overcome by using nanoformulation technologies, a process that involves a polymeric particle matrix that carries pesticide molecules inside.[4] The loaded pesticide is then released in a controlled manner in response to external stimuli. The synthesis of hollow mesoporous silica (HMS) with scalable structures and different synthesis mechanisms[5,6] and properties[7,8] has stimulated significant attention in the last several decades. HMS containers have multilateral intrinsic characteristics, such as excellent biocompatibility,[9,10] high stability,[11] high loading capacity, and non-immunogenicity. In addition to its capability of encompassing a gatekeeper on the outer surface,[12−16] being nontoxic to living cells[17] is its most environmentally valuable feature. Since the first gated silica mesoporous particle was developed,[18] a variety of such systems of silica nanoparticles with stimuli-responsive gatekeepers have been presented to control the release of drug molecules in restraint of outward stimulators, such as light,[19−21] redox potential,[22,23] pH,[24] and enzymes.[25−28] Further systems, including pseudorotaxanes,[29] carboxylates,[30] and complexes such as cyclodextrin,[31] cucurbit[6]uril,[32] and cucurbit[7]uril,[33] have also been prepared. In addition, additional preliminary studies that use alternate exterior stimuli, such as temperature[34] and the presence of specific anions,[35] have also been reported. Countless nanocarriers had been synthesized for the delivery of pesticides, such as polymeric nanospheres,[36−38] microcapsules,[39−43] solid lipid nanoparticles,[44,45] layered double hydroxides and clays,[46−49] nanosized metals and metal oxides,[50] and carbon nanotubes.[51] Nevertheless, programmed silica nanocontainers that are capable of pH and enzyme responsive release of pesticide molecules are currently under intensive investigation.[52,53] This not only can strengthen some active ingredients (AI) to withstand deterioration factors that may adversely affect the active substances performance but can also prolong the AI bioavailability.[54] Chlorantraniliprole (CLAP) is a new compound that belongs to the family of anthranilic diamides as selective insecticides and presents a novel mode of action by stimulating the insect ryanodine receptors (RyRs). CLAP in water can be deteriorated by both chemical and photochemical procedures.[55] One goal is to utilize the advantage of carbohydrate digestion and the digesting technique in pesticide formulation technology. α-Cyclodextrin (α-CD) is a cyclic oligosaccharide composed of α-(1,4) linked glucopyranose subunits that can be enzymatically hydrolyzed by α-amylase. Whereas enzymes are assimilation keys and exist in any digestive system, α-amylase is our liberation key that exists in the salivary glands and midgut of larvae with chewing mouthparts.[56,57]

Orienting the pesticide particles to be released inside a specific group of insects is a new promising research field in pesticide formulation science that depends on the insect's feeding type. In particular, insects that eat plant leaves may be specifically

Received: June 2, 2017
Revised: July 29, 2017
Accepted: August 15, 2017
Published: August 15, 2017

DOI: 10.1021/acs.jafc.7b02560
J. Agric. Food Chem. 2017, 65, 7854−7864

targeted because most of their natural enemies are not vegetarian. Moreover, by using a formulation with segregation, the natural enemies of the target insects may be kept far from the application. In addition, this decreases the interaction between the pesticides and the ecosystem. The reported research suggests that enzymatic degradation of HMSs α-CD gatekeepers is a suitable record for the on-command delivery of the active ingredient of the pesticide. Moreover, the chance of using an enzyme for differentiated pesticide release unlocks an enormous variety of new standpoints in the development of biocompatible pesticide delivery systems. Nevertheless, to the best of the authors' knowledge, examples of enzyme-induced pesticide delivery systems using mesoporous silica nanoparticles are still in the earliest stages of development.

The theme of this study is the synthesis of surface functionalized HMS nanoparticles, with different sizes and various release profiles, which are enzymatically *in vivo* uncapped and allow the cargo to be released in an insect's midgut. The synthesized surface functionalized HMS nanoparticles were utilized as CLAP carriers, which will assist environmentally in agricultural pest control.

MATERIALS AND METHODS

Materials. 2,2′-Azobis(isobutyronitrile) (AIBN), 2,2′-azobis(2-methylpropionamidine) dihydrochloride (V-50, > 97.0%), styrene (St, > 99.0%, stabilized with TBC), hexadecyltrimethylammonium bromide (CTAB, > 99.0%), ammonium hydroxide solution (28 wt %), polyvinylpyrrolidone (>99.5%) K30 average Mw 40.000, [2-(Acryloyloxy) ethyl] trimethylammonium chloride solution (AETAC, 80 wt % in water), and 2-propanol (>99.9%) were obtained from Sino pharm Chemical Reagent Co., Ltd. *N*-Phenylaminopropyltrimethoxysilane (PhAPTMS 96%), α-cyclodextrin (α-CD 98%) and α-amylase (enzyme activity is 50 μmol mg^{-1} min^{-1}) were obtained from Heowns Biochem Technologies. Llc. Methanol (MeOH > 99.9%), toluene (PhMe > 99.5%), ethanol (95%), acetone (99.5%), ethanol (99.9%), and Tetraethyl orthosilicate (TEOS > 99.9%) were obtained from Tianjin and Aladdin Reagent (Shanghai) Co., Ltd. All chemicals were used without additional purification. Deionized water was generated with Sartorius Stedim arium pro-Ultrapure Water System.

Synthesis of CLAP-CRFs. Three HMSs with different sizes, denoted as HMS 140, HMS 400, and HMS 1500, where the number indicates the mesoporous nanoparticles' external diameter, were synthesized[58] with our modifications that are well-defined in the Supporting Information. In an aqueous solution of ammonium hydroxide, HMSs were synthesized in a weakly basic water/ethanol medium using a comparatively concentrated polystyrene template. In the presence of weak basicity and a suitable ratio of ethanol/water, exact control of the tetraethyl orthosilicate (TEOS) hydrolysis rate can be achieved, which, together with the high concentration of PS latex, decreases the opportunity of forming solid mesoporous particles as well as combining them together. For synthesizing 400 HMS at 40 °C, PS latex (5.74 wt %) with a size of approximately 400 nm have been added dropwise to a solution containing water (19.48 wt %), hexadecyltrimethylammonium bromide (CTAB) (1.62 wt %), ethanol (22.32 wt %), and ammonium hydroxide (2.77 wt %) under vigorous stirring. Then, the mixture was sonicated for 120 min and followed by magnetic stirring for 30 min before adding TEOS (3.044 wt %) dropwise. The mixture was then kept at 40 °C for 48 h before the mesoporous silica coated PS latex was gathered by centrifugation and washed thrice with ethanol. The PS templates were removed through calcining in air at 600 °C for 8 h. HMS 140 and HMS 1500 were synthesized in a parallel method using the suitable size of PS latex.

HMS surface functionalization. The three sizes of HMSs were surface functionalized with PhAPTMS to achieve a phenylamine functionalized silica surface. One g of each HMS sample was treated with linker molecules (0.27 mL of PhAPTMS) in dry PhMe (100 mL) and left for 24 h to reflux under N_2. The surface functionalized HMSs were filtered, and washed with PhMe and MeOH thrice, then dried in a vacuum oven at 60 °C for 24 h.

Loading CLAP cargo molecules and sealing HMS pores. *N*,*N*-Dimethylformamide/CLAP solution (AI/DMF 0.124 gmL^{-1}), were loaded into the nanopores by diffusion for 24 h at RT. Then, the CLAP loaded PhAP-HMS were collected by centrifugation followed by washing thrice with methanol and drying under vacuum at 60 °C for 24 h. Drug loading efficiency was calculated per the following equation:

$$\text{Drug loading efficiency (\%)} = 100 \times (W\ loss^{CLAP\text{-}CRF} - W\ loss^{\alpha\text{-}CD\text{-}PhAP\text{-}HMS})$$

Finally, by sealing the CLAP loaded PhAP-HMS with α-CD, a surplus amount of α-CD was dissolved in an aqueous solution. Then, 0.20 g of CLAP loaded PhAP-HMS was added, followed by sonication and stirring at RT for 3 days. Finally, the samples were washed with water until no dye was detected in the washing solution. The capped nanoparticles were subsequently dried at 75 °C for 24 h.

Characterization. The morphology and structure of the HMS samples were characterized using a transmission electron microscope (TEM); images were collected on a JEM-2100F instrument. Scanning electron microscope (SEM) images were collected on an SU8200 instrument, all SEM samples were coated by gold dust. A Fourier transform infrared spectroscopy (FT-IR) VORTEX70 instrument was used to observe the chemical grafting processes occurring with the HMSs. The drug loading efficiency (DLE), determined by the weight lose of the HMS materials, was determined with a Pyrisl TGA thermogravimetric analyzer (TG-TDA). Size distribution was measured by DLS (dynamic light scattering) using a zetasizer (Zetasizer Nano ZS, Malvern Co., U.K.). N_2 adsorption−desorption isotherms were conducted at 77 K on a Micromeritics ASAP 2460 analyzer (Micromeritics Instrument Corporation, USA) under continuous adsorption conditions. The BET model was performed to estimate the specific surface areas. From the adsorption data by using BJH method pore size and pore volume were determined. The analysis of the released CLAP from CLAP-CRF was quantified with high-performance liquid chromatography (HPLC) with the following HPLC conditions. The chromatographic column was C_{18} (25 cm length, 4.6 mm inner diameter, and 4.0 μm particles). A mixture of 0.01% formic acid in water and methanol (40:60, v/v) served as the CLAP mobile phase. A flow rate of 1.0 mL min^{-1} was used, along with UV detection at a wavelength of 265 nm, and 20 μL was set to be the injection volume for all samples and standards with a run time of 15 min.

CLAP-CRFs thermal and light stability assay. The shelf life for a pesticide is the period that any pesticide can be stockpiled before it deteriorates. Nearly all pesticides have a limited shelf life. As a part of modern pesticide formulation technologies, packing procedures and storage practices aim to extend the shelf life as much as possible. The active ingredient might change chemically and collapse into sub products that may no longer have toxicological properties, consequently decreasing the original active ingredient concentration. To investigate the thermal stability, 0.20 g from the obtained CRFs was packed and stored in Pyrex dark glass tubes at 40, 50, and 60 °C for a period of 60 days. The active ingredient alterations were analyzed by HPLC to determine the deterioration effects on the wrapped CLAP molecules. CRFs UV-shielding properties were also examined; 0.20 g from each CRF was mixed with 500 mL of an acetone−H_2O mixture (30:70, v/v), then transferred to a 1000 mL cylindrical reaction vessel with a magnetic stirrer. The samples were exposed to a 36 W germicidal lamp (254 nm) at 20 cm, and the temperature was adjusted to RT. Then, 2 mL of the mixture was sampled with a Digital SLP Cell Disruptor (SLPt time, Emerson Electric Co., USA) at different periods, followed by centrifugation and using the supernatant to perform HPLC analysis to determine the active ingredient changes compared with the technical grade CLAP that was used as a control in the test.

Statistical analysis of controlled release data. All quantitative trials were carried out in triplicate. the mean values with standard deviations were calculated. The results are expressed as (mean ± SD) calculated by using (SPSS version 24).

DOI: 10.1021/acs.jafc.7b02560
J. Agric. Food Chem. 2017, 65, 7854−7864

Scheme 1. Synthesis Steps of CLAP-CRFs[a]

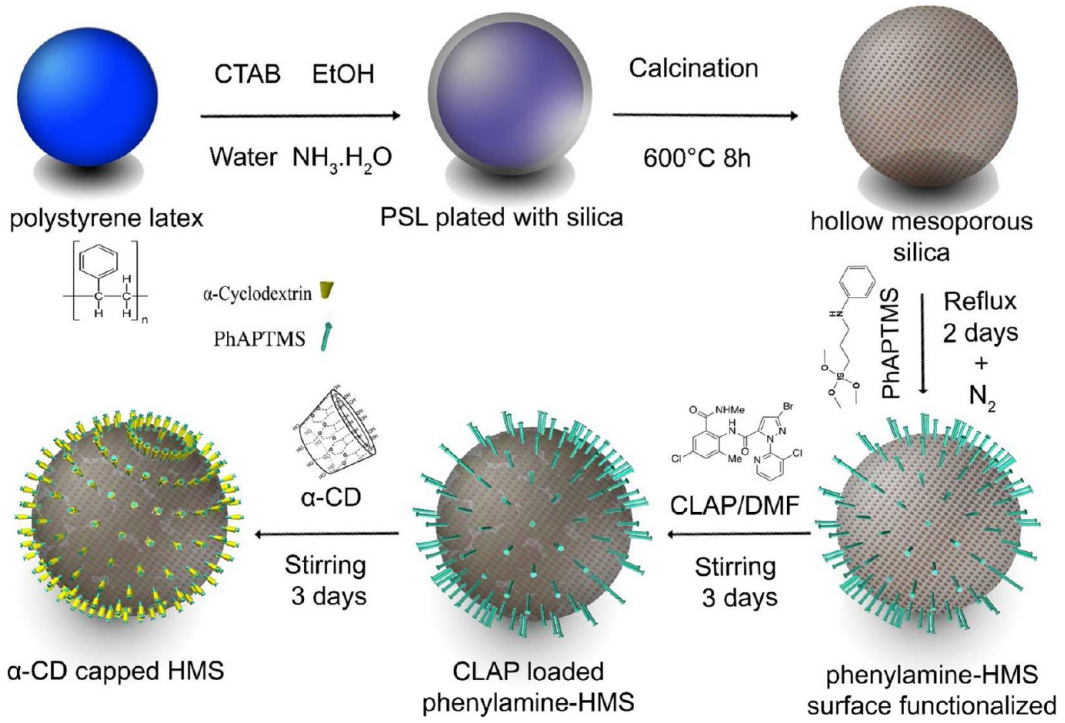

[a]Starting with the synthesis of PS latex with different diameters, then polycondensation of hydrolyzed TEOS in the presence of CTAB surfactant, ammonium solution, and ethanol. The gathered PSL coated with silica followed by calcination to remove the PS template. The obtained HMSs treated with PhAPTMS to achieve phenylamine surface functionalized HMSs, followed by the CLAP/DMF solution diffusing into HMSs internal space and then, finally, capping with α-CD.

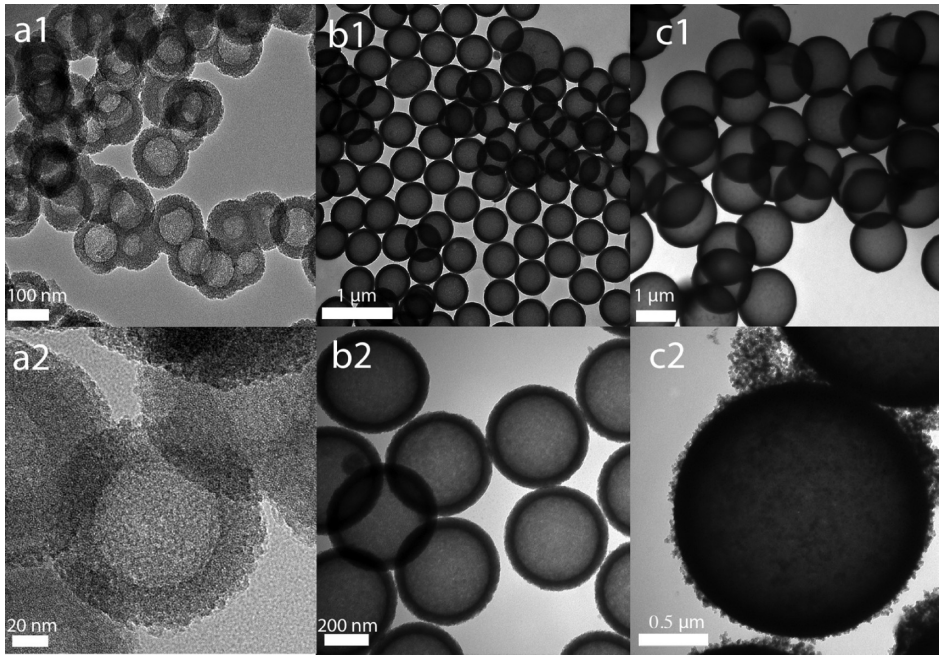

Figure 1. TEM images for (a1) 140 nm HMS, (b1) 400 nm HMS, (c1) 1500 nm HMS, (a2) 140 nm CLAP-CRF, (b2) 400 nm CLAP-CRF, and (c2) 1500 nm CLAP-CRF.

CLAP release figuration from CLAP-CRF under various stresses. 500 mL of dissolution tester D-800LS in an acetone−H_2O medium (30:70, v/v) was prepared to disband CLAP from the CRFs. A fixed amount 0.20 g from CLAP-CRFs were dispersed in the medium and kept under 100 rpm stirring. At pH 7, the impact of size differentiation on the release behavior was investigated. Next, 400 nm CLAP-CRF was selected as a model formulation to evaluate the release behavior under different pH values 5, 7, and 10, temperatures at 25 °C, 35 °C, and 45 °C and in the presence or absence of the α-amylase enzyme. In the release medium, the CLAP cumulative release values were calculated, 2.0 mL aliquots were collected at regular periods from the dissolution tester suspension. Centrifugation at 10000 rpm was

DOI: 10.1021/acs.jafc.7b02560
J. Agric. Food Chem. 2017, 65, 7854−7864

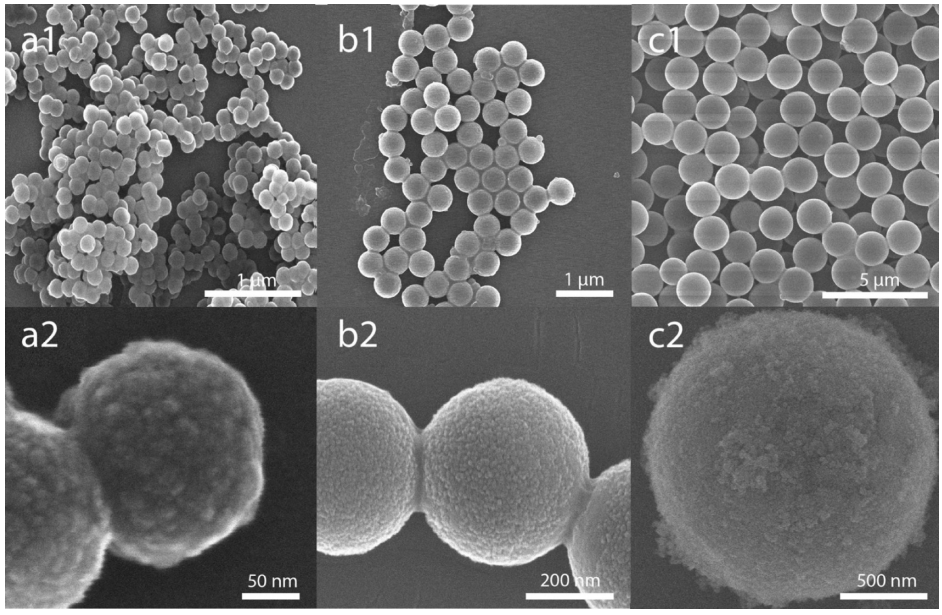

Figure 2. SEM images for (a1) 140 nm HMS, (b1) 400 nm HMS, (c1) 1500 nm HMS, (a2) 140 nm CLAP-CRF, (b2) 400 nm CLAP-CRF, and (c2) 1500 nm CLAP-CRF. All samples were coated by gold dust.

carried out to obtain 50 μL of supernatant that lacked CRF particles for HPLC analysis using the mentioned method above, and the remaining mixture was returned to the test flask.

CLAP-CRFs biological activity survey. Freshly hatched and reared larvae of the diamondback moth, *Plutella xylostella*, were kept at RH (60 ± 5) %, (28 ± 1) °C, and 14L:10D, and were nourished with a diet of *Brassica rapa* cabbage seedlings. The third instar larvae were then nourished on fresh *Brassica rapa* leaves grown for 60 days under field conditions to emulate nature conditions without any agrochemical treatments. A stock solution of all formulations (25.0 mg L^{-1}) was prepared by dispersing the pesticide formulation in water. The plants were grouped into the commercial formulation (Coragen) group and the CRF group. The leaves were gathered at various sequential harvests at 0, 1, 3, 5, 7, 10, and 14 days after the formulations were spread. Biological activity data analysis was studied then LC_{50} and LC_{90} was calculated by applying the regression Chi-squared test equation:

$$Y = a + bX$$

where Y = probit value corresponding to 50% response, X = the Log dosage, a = intercept, and b = slope.

RESULTS AND DISCUSSION

Scheme 1 shows the preparation and synthesis of CLAP-CRFs which was performed in six steps. Figure 1 shows TEM images confirming the successful synthesis of HMSs. The synthesized HMS images indicate the presence of hollow silica spheres, which formed after the calcification of the silica spheres. TEM images indicate excellent particle symmetry, and nearly all of the HMS had a hollow shape with a smooth shell. The electron contrast between the cores and the shells confirms the formation of hollow particles. The average shell thicknesses of HMS 140, 400, and 1500 are 23, 25, and 63 nm, respectively. Figure 2 (a1, b1, and c1) shows the SEM investigation which exhibits that the mesoporous silica nanoparticles have excellent spherical morphologies. Figure 2 (a2, b2, and c2) displays the surface after phenyl amine functionalization and α-CD caps, which gives a visual confirmation of surface morphology modification.

Figure 3 displays the FT-IR spectra of a sample of blank HMS, the phenylamine surface functionalized HMS (PhAP-HMS), CLAP loaded PhAP-HMS, and α-CD capped CLAP loaded

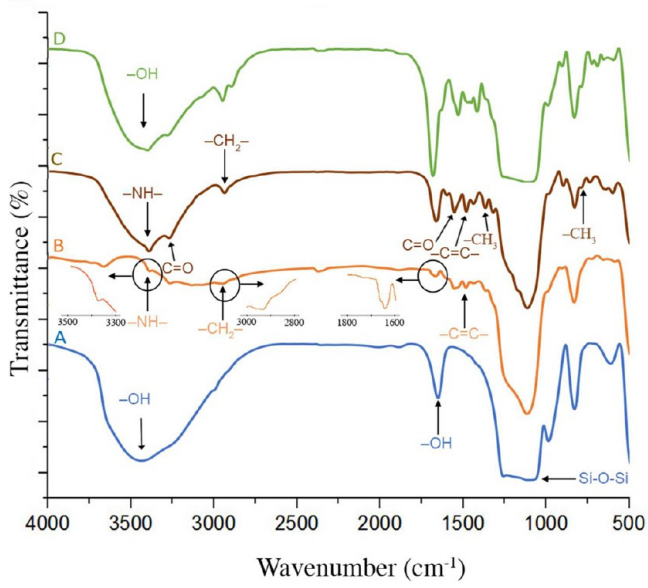

Figure 3. 400 nm CRF FT-IR spectra of (A) blank HMS, (B) PhAP-HMS, (C) CLAP loaded PhAP-HMS, and (D) CLAP-CRF. KBr was used as a background.

PhAP-HMS. For the blank HMS sample, the vibration bands characteristic of (−OH) stretching appear at 3436 cm^{-1}, and the sharp peaks at 1084 cm^{-1} can be attributed to the stretching vibrations of the mesoporous structure (Si−O−Si) (Figure 3A). The spectrum of PhAP-HMS (Figure 3B) reveals a new absorption band of the alkanes group ($-CH_2-$) from 2934 to 2941 cm^{-1}. In addition, the stretching vibration peak of the aliphatic amine group (−NH−) appears at 3420 cm^{-1}. The vibration peaks of aromatic hydrocarbons (−C═C−) appear at 1499 to 1508 cm^{-1}. These results indicate that the phenylamino silane group of PhAPTMS successfully reacted with the surface hydroxyl group of the HMSs. The CLAP loaded PhAP-HMS (Figure 3C) displays a much stronger absorption band at 3389 cm^{-1} because of CLAP (−NH−) stretching. It also shows higher

DOI: 10.1021/acs.jafc.7b02560
J. Agric. Food Chem. 2017, 65, 7854−7864

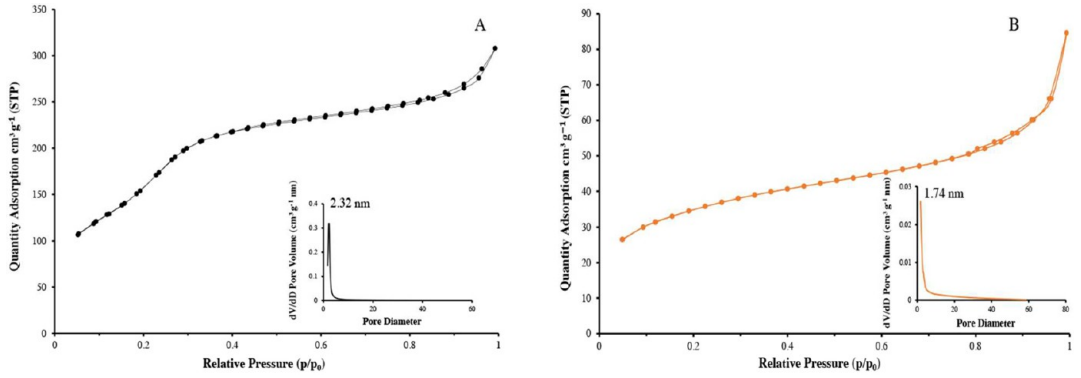

Figure 4. Nitrogen adsorption−desorption isotherms for (A) HMS 400 and (B) α-CD-HMS 400. Insets: Pore size distribution of each HMS and α-CD-HMS.

absorption peaks at 1389 cm^{-1} and 795 cm^{-1} due to the significant increase of asymmetrical stretching from the CLAP methyl groups (−CH_3). Furthermore, the absorption band of the CLAP aliphatic ketone group (C═O) appears at 1716 cm^{-1}, and over tuning at 3350 cm^{-1}, and the absorption bands of the aromatic hydrocarbons (−C═C−) stretch occur at 1453 cm^{-1} to 1457 cm^{-1}, demonstrating that CLAP has been incorporated into the HMSs. α-CD capped CLAP loaded PhAP-HMS (Figure 3D) displays broadened peak shape at 3387 cm^{-1}, which is related to the α-CD (−OH) group (Supporting Information Figures S1−S4).

The N_2 adsorption−desorption isotherm of the HMS 400 nm (Figure 4) is qualitatively like the isotherms of HMS 1500 nm and HMS 140 nm (Figure S5 and S6 in the Supporting Information). Both exhibit a type IV isotherm typical for mesoporous material. The adsorption step ascribed to the mesopores and the pore texture preserves an appreciable decrease in the N_2 volume adsorbed for HMS 140, 400, and 1500 nm (BJH mesopore volume = 0.42 $cm^3\ g^{-1}$, 0.31 $cm^3\ g^{-1}$, 0.31 $cm^3\ g^{-1}$), respectively. The surface area was measured ($0.711 \times 10^3\ m^2\ g^{-1}$, $0.654 \times 10^3\ m^2\ g^{-1}$, and $0.102 \times 10^3\ m^2\ g^{-1}$), respectively. The surface area of solid α-CD capped HMS was reduced about 70%, when compared to that presented by blank HMS, due to the external grafting of α-CD. As observed for blank HMS, the BJH pore size distribution shows a maximum at 2.32, 2.38, and 2.46 nm for the three sizes respectively on the border between mesopores and micropores. On the other hand, the adsorption step at high relative pressure ($P/P_0 > 0.8$), which appears in the isotherm of HMS, and α-CD capped HMS can be estimated. For blank HMS, 140, 400, and 1500 nm, the BJH N_2 adsorption was (0.78 $cm^3\ g^{-1}$), (0.46 $cm^3\ g^{-1}$), and (0.38 $cm^3\ g^{-1}$), respectively, whereas for α-CD capped HMS, the BJH N_2 adsorption was (0.09 $cm^3\ g^{-1}$), (0.14 $cm^3\ g^{-1}$), and (0.22 $cm^3\ g^{-1}$), respectively. These data support the fact that the α-CD caps are specifically incorporated on the pores rims of the ordered mesopores. BET specific surface values, pore volumes, and pore sizes calculated from the N_2 adsorption−desorption isotherms for HMS 140, HMS 400, HMS 1500, α-CD capped HMS 140, α-CD capped HMS 400, and α-CD capped HMS 1500 are listed in Table 1.

Figure 5 shows HMS particles size distribution. The sizes fluctuated from 118 to 190 nm, 371 to 476 nm, and 1342 to 2670 nm for the three HMS samples, with middle sizes of 140, 400, and 1500 nm, respectively. These results were confirmed by TEM images.

Table 1. Properties of HMS and α-CD Capped HMS Calculated from N_2 Adsorption−Desorption Isotherms

Sample	S_{BET} ($m^2\ g^{-1}$)	BJH pore size (nm)	BJH Pore volume ($cm^3\ g^{-1}$)
HMS-140 nm	0.711×10^3	2.32	0.42
HMS-400 nm	0.654×10^3	2.38	0.31
HMS-1500 nm	0.102×10^3	2.46	0.31
α-CD capped HMS 140 nm	0.117×10^3	1.74	0.02
α-CD capped HMS 400 nm	0.190×10^3	1.74	0.02
α-CD capped HMS 1500 nm	0.040×10^3	1.74	0.06

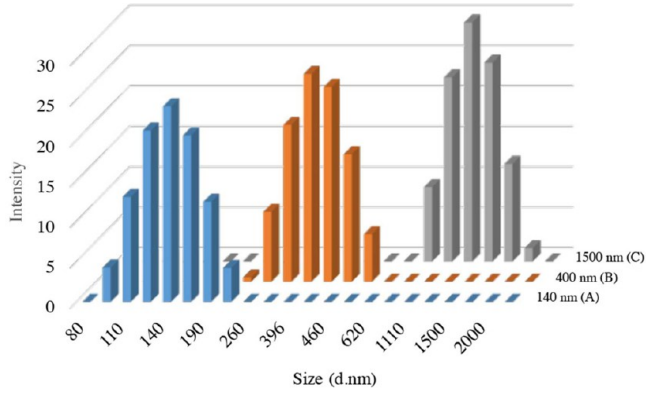

Figure 5. Dynamic light scattering (DLS) of obtained HMS nanoparticles: (A) 140 nm HMS, (B) 400 nm HMS, and (C) 1500 nm HMS (dispersed in EtOH).

Furthermore, the drug loading efficiency (DLE) and the decomposition of CLAP-CRF, α-CD capped PhAP-HMS, and hollow HMSs were determined by thermogravimetric analysis (TGA). Figure 6 presents TGA results showing that the decomposition of α-CD starts at 518 K and the CLAP decomposition starts at 514 K. Hollow HMSs have a decrease in total weight due to vapor volatilization (4.96% from the total weight). In contrast, hollow capped HMSs with α-CD total weight loss have a slight increase over the weight loss for hollow HMSs (7.91% from the total weight) due to the presence of the α-CD coating. The 140, 400, and 1500 nm CRFs showed significant weight decreases of 50.1%, 46.2%, and 41.5%, respectively, which were attributed to the loaded amount of CLAP. In contrast, the exact loaded amounts of CLAP into the HMSs were 42.22%, 38.29%, and 33.66%, respectively, with

DOI: 10.1021/acs.jafc.7b02560
J. Agric. Food Chem. 2017, 65, 7854−7864

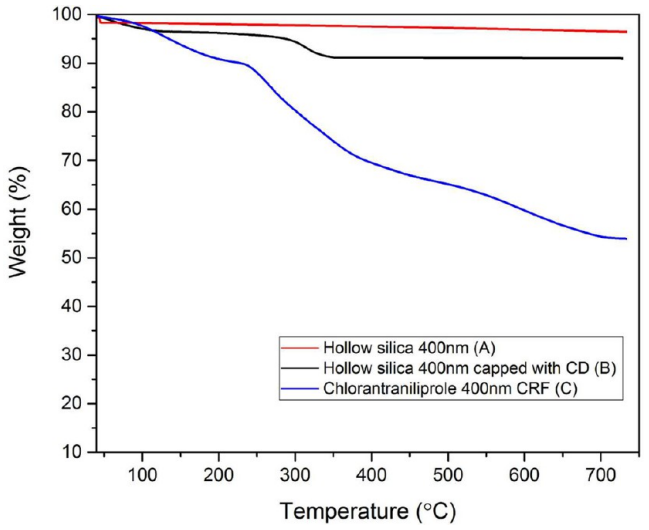

Figure 6. TGA curves for (A) hollow silica 400 nm HMS, (B) α-CD capped 400 nm PhAP-HMS, and (C) 400 nm CLAP-CRF.

respect to the total weight of the HMSs (Supporting Information Figures S7−S10).

A series of distilled water samples at various pH values and temperatures and in the presence or absence of α-amylase were prepared to study the release behavior of different CRFs under different stresses. A 100-rpm stirring rate, pH 7, and room temperature (RT) were the adjusted conditions to investigate the effect of size differentiation, various pH values, and the presence or absence of α-amylase enzyme on the release behavior. Figure 7

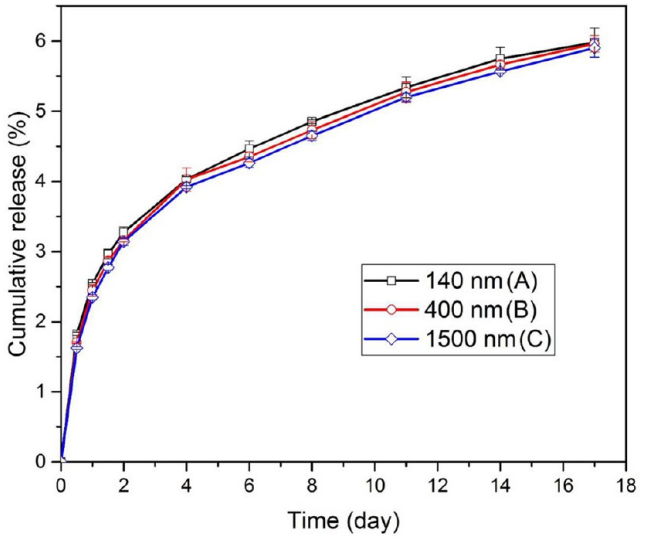

Figure 7. Controlled release profile for different CRF sizes: (A) 140 nm, (B) 400 nm, and (C) 1500 nm at pH 7 at RT and 100 rpm stirring rate (mean ± SD, n = 3 for each sample).

depicts release profiles for the three particle sizes. The cumulative release rates of 140, 400, and 1500 nm CLAP-CRFs were 6.0%, 5.9%, and 5.8% on the 17th day, respectively. In this study, the release profiles of all HMS sizes have a low initial release rate (approximately 6%). The bursting CLAP release could be assigned to the desorbed CLAP molecules on the HMSs surface due to the hydrogen bonding between CLAP molecules and the HMS surface. This means that the nanomaterials showed a residual release of about 6% in the absence of any stimuli. Our results agreed with previous studies.[25−28]

Figure 8 displays the influence of pH values 5, 7, and 10 on the cumulative release rates of the 400 nm CRF sample. At pH values

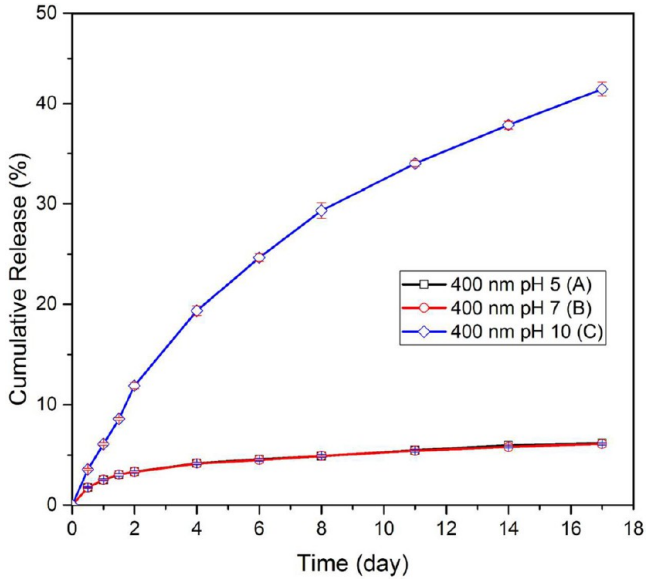

Figure 8. Influence of (A) pH 5, (B) pH 7, and (C) pH 10 on the cumulative release profile of 400 nm HMS at RT and 100 rpm stirring rate (mean ± SD, n = 3 for each sample).

5, 7, and 10, the release rates were 4.19% to 6.16%, 4.04% to 5.96%, and 19.30% to 41.56%, respectively, from the 4th day to the 17th day. The release of CLAP at pH 5 and 7 is slower compared with the rate at pH 10. The cumulative release was amplified at pH 10, which was probably due to the basic pH effect on the HMS. Si−O−Si bonds hydrolyzed more easily at a raised pH after the same elapsed period for the other pH values. Additionally, at pH 5 and pH 7, a leisurely CLAP release occurs from the 400 nm CRF that cannot be attributed to the trapped CLAP because of the pores sealing to prevent CLAP release from the CRFs, whereas the detected CLAP is assigned to the desorbed molecules on the HMS surface.

Additionally, 25 °C, 35 °C, and 45 °C were the variable factors for investigating the 400 nm CLAP-CRF release behavior under different temperatures. Figure 9 elucidates that the release rates at 25 °C, 35 °C, and 45 °C sequentially were 4.04%, 4.76%, and 5.68% at day 4, and 5.96%, 7.46%, and 9.18% at day 17. It was incidental that the release rates progressively become quicker as the temperature increased. This was basically attributed to the thermal effect on α-CD, leading to destabilize its structure, which resulted in an easier and faster CLAP release from the CRF at a higher temperature.[59]

Experiments were conducted to inspect the capability of shielding the CRF active ingredient against UV radiation and storage at different temperatures. Three CRFs (140, 400, and 1500 nm) and technical grade CLAP were subjected to this test. CLAP-CRFs and technical grade CLAP were kept at 40 °C, 50 °C, and 60 °C for 60 days. HPLC was used to observe the active ingredient changes with the method described previously. Table 2 displays that CLAP molecules in CRFs under high temperatures are more stable than is the technical grade CLAP. The decomposition rate of enfolded CLAP in all CRF samples was much lower than that of technical CLAP, which revealed more

DOI: 10.1021/acs.jafc.7b02560
J. Agric. Food Chem. 2017, 65, 7854−7864

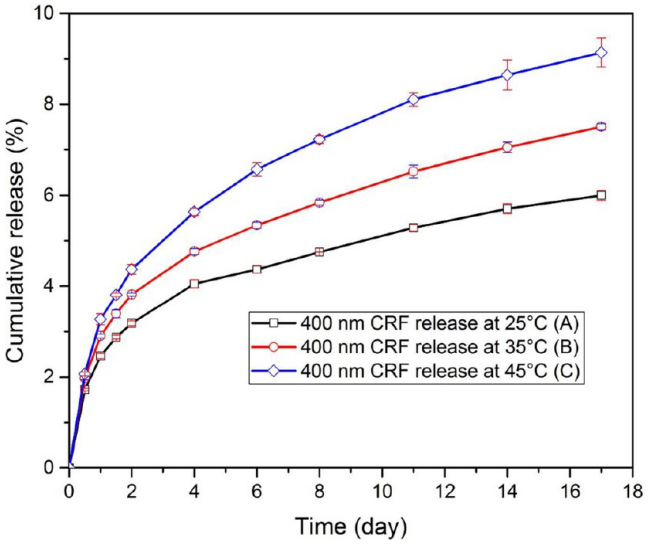

Figure 9. 400 nm CLAP-CRF release behavior at (A) 25 °C, (B) 35 °C, and (C) 45 °C at pH 7 and 100 rpm stirring rate (mean ± SD, n = 3 for each sample).

than 98% decomposition after 3 h of UV radiation. Moreover, after 24 h of UV radiation, the decomposition rate of enfolded CLAP in CRFs was less than 10%. The obtained data establish that CLAP can be preserved by the CRFs shell and represent an outstanding UV-shielding capability for the synthesized CLAP-CRFs.

The cargo release system is reliant on the gatekeepers, which are based on the inclusion complex formed by α-CD with PhAP group interactions. When α-CD interacts with the PhAP groups attached on the HMS pore orifices through silanol groups, the inclusion complexes act as stoppers to prevent cargo release. In the presence of α-amylase, α-CD can be hydrolyzed to glucose monomers, leading to cargo release (Scheme 2). To confirm the proposed α-amylase enzyme stimulus response facilitated by the gatekeeper mechanism, a 100-rpm stirring rate and pH 7 at RT were the constant conditions for investigating the 400 nm CLAP-CRF release behavior in the presence or absence of α-amylase enzyme (0.65 mg mL^{-1}). The release behaviors were paralleled until day 4, when the α-amylase solution that uncapped the CRF was added, which led to rapid release. Figure 10 presents the impact of the presence of α-amylase enzyme on the cumulative release rate of 400 nm CRF. The release behavior in the absence of enzyme was 4.04% to 5.96% from the 4th day to the 17th day.

Scheme 2. Schematic Diagram of CLAP Release from the CLAP-CRF after α-CD Hydrolysis by α-Amylase

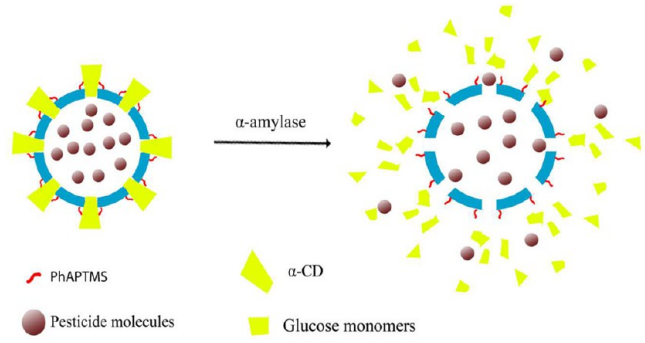

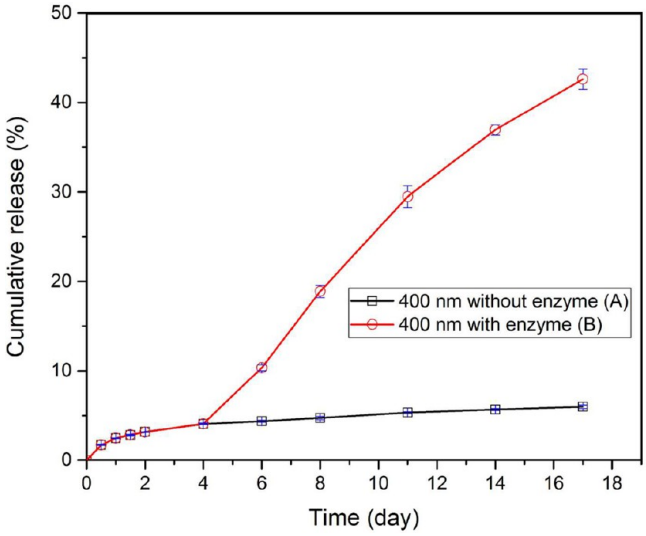

Figure 10. Influence of the presence or absence of α-amylase enzyme (0.65 mg mL^{-1}) on the cumulative release rates: (A) 400 nm release without enzyme; (B) 400 nm release with the enzyme at RT, pH 7, and 100 rpm stirring rate (mean ± SD, n = 3 for each sample).

In contrast, the release behavior in the presence of α-amylase was 4.05% to 42.47% in the same elapsed time. This proves that the CRFs selectively unsealed in the presence of α-amylase by the rupture of α-CD α-1,4 bonds between the glucose monomers. α-Amylase hydrolyzes the alpha bonds of large α-linked polysaccharides, such as α-CD, yielding glucose monomers. In

Table 2. CLAP-CRF Stability under UV Radiation and Different Temperatures

Tests at different conditions	Decomposition rate (%)			
	CLAP technical grade	140 nm	400 nm	1500 nm
Irradiation at 254 nm for 1 h	32.17	2.57	2.55	2.49
Irradiation at 254 nm for 2 h	53.26	3.31	3.28	3.27
Irradiation at 254 nm for 3 h	72.84	3.99	3.99	3.92
Irradiation at 254 nm for 4 h	91.58	4.72	4.73	4.69
Irradiation at 254 nm for 6 h	100	5.55	5.51	5.49
Irradiation at 254 nm for 12 h	100	6.48	6.45	6.45
Irradiation at 254 nm for 18 h	100	7.62	7.58	7.55
Irradiation at 254 nm for 24 h	100	8.53	8.49	8.47
Storage 60 days at 40 °C	3.97	1.02	1.02	0.99
Storage 60 days at 50 °C	7.82	1.95	1.93	1.92
Storage 60 days at 60 °C	13.25	3.63	3.61	3.61

DOI: 10.1021/acs.jafc.7b02560
J. Agric. Food Chem. 2017, 65, 7854−7864

Table 3. Evaluation of Different Concentrations from CLAP-CRF and Coragen on *P. xylostella* Mortality at *Brassica rapa* in Different Picking Times

Conc of treatment (mg L^{-1})		Mortality (%)						
		Day 0	Day 1	Day 3	Day 5	Day 7	Day 10	Day 14
CLAP-CRF	0.05	46.67	46.66	40.00	40.00	36.67	36.66	33.33
	0.1	83.33	76.66	66.67	56.67	50.00	46.66	43.33
	0.4	90.00	86.67	80.00	80.00	66.67	56.66	53.33
	0.8	96.67	93.33	90.00	90.00	83.33	73.33	73.33
	1.2	100	100	100	100	96.67	93.33	93.33
Coragen	0.05	40.00	26.67	26.67	6.66	3.33	3.33	3.33
	0.1	53.33	46.67	46.67	43.33	33.33	16.66	13.33
	0.4	73.33	60.00	56.67	46.67	43.33	30.00	26.66
	0.8	83.33	76.67	73.33	63.33	60.00	50.00	43.33
	1.2	100	96.67	90.00	86.67	76.66	70.00	66.66

Table 4. Constants from Fitting the Chi-Squared Equation, $y = a + bx$, for the Biological Activity Data of CLAP-CRF and Coragen on Different Days

Time after spraying (day)		LC_{50} (mg/L, 95% fiducial limit)	LC_{90} (mg/L)	Slope (mean ± SE)	Chi-square value
CLAP-CRF	Day 0	0.039 (0.018−0.085)	0.31	1.46 ± 0.17	3.24
	Day 1	0.042 (0.018−0.097)	0.47	1.22 ± 0.18	1.80
	Day 3	0.064 (0.029−0.143)	0.80	1.16 ± 0.17	1.15
	Day 5	0.078 (0.037−0.164)	0.84	1.23 ± 0.16	5.56
	Day 7	0.109 (0.056−0.215)	1.21	1.21 ± 0.15	3.03
	Day 10	0.134 (0.061−0.295)	2.60	0.99 ± 0.17	4.70
	Day 14	0.156 (0.074−0.329)	2.54	1.06 ± 0.16	5.27
Coragen	Day 0	0.088 (0.036−0.212)	1.73	0.98 ± 0.19	3.50
	Day 1	0.152 (0.081−0.285)	1.54	1.27 ± 0.13	4.92
	Day 3	0.169 (0.080−0.356)	2.46	1.10 ± 0.16	3.12
	Day 5	0.305 (0.167−0.559)	2.90	1.30 ± 0.13	9.32
	Day 7	0.423 (0.235−0.763)	3.86	1.33 ± 0.13	5.81
	Day 10	0.674 (0.365−1.245)	5.26	1.44 ± 0.13	2.30
	Day 14	0.824 (0.433−1.568)	6.57	1.42 ± 0.14	2.15

insects, α-amylase is present in salivary glands and midgut, which works as the key for pesticide release from HMSs.

The remarkable enzyme sensitivity and excellent photothermal stability of CLAP-CRFs highlight their great potential in targeting pesticide release. After the positive demonstration of CLAP-CRF release kinetics with different release profiles, there was a strong eagerness to examine the toxicity of CLAP-CRF *in vivo*. To evaluate the biological activity of the formulation, the third instar of *P. xylostella* was selected as a model insect and 400 nm CRF was selected as a model formulation to perform the biological activity survey. The CLAP active ingredient LC_{90} was calculated using the (SPSS version 24) statistic software, and the resulting LC_{90} was 1.1459 mg L^{-1}. 400 nm CLAP-CRF was compared with the Coragen and CLAP-free CRF. As a model plant, two hundred *Brassica rapa* plants were grown. Ten groups of plants were selected, with three replicates for each group. Each selected plant was required to have at least seven leaves (one leaf for each harvest). Ten third instar larvae of *P. xylostella* were set for each replicate. Five ascending concentrations were defined as 0.05, 0.1, 0.4, 0.8, and 1.2 mg L^{-1} for both CLAP-CRF and Coragen. Seven picking days were defined, day 0, day 1, day 3, day 5, day 7, day 10, and day 14, to evaluate the biological effects of CLAP-CRF compared with Coragen and CLAP-free CRF. We name the method as "regular sampling feeding experiment". Table 3 presents the derived biological activity survey results. The Chi-square equation was used for fitting. LC_{50} and LC_{90} values of CLAP-CRF were calculated and are offered in Table 4. In CLAP-free CRF at 1.2 mg L^{-1}, no larvae died. Moreover, it was observed that the surviving insects' activity in the CLAP-CRF treated trials was very weak due to CLAP imparting muscle regulation, which caused larvae paralysis. In addition, the chewing spots do not suggest continuous feeding. The mortality was high at day 0 for all CLAP-CRF treatments, starting with 50% mortality for 0.05 mg L^{-1} and up to 100% mortality for 1.2 mg L^{-1}, paralleled with Coragen, which started with 30% mortality for 0.05 mg L^{-1} and up to 100% at 1.2 mg L^{-1}. For day 1, the mortality slightly decreased for all treatments, down by 3.33% of Day 0 at CLAP-CRF 0.05 mg L^{-1} compared with Coragen 0.05 mg L^{-1}, which kept the same Day 0 mortality. For CLAP-CRF 0.1 mg L^{-1} and 0.4 mg L^{-1}, the mortality values were 76.66% and 86.66% at day 1, respectively, which were much higher compared with 0.1 mg L^{-1} and 0.4 mg L^{-1} Coragen. The CLAP-CRF mortality at day 3 decreased in all concentrations but was still higher compared with Coragen on the same day. At day 5 Coragen 0.05 mg L^{-1}, mortality decreased from 26.6% to 6.66%, which is attributed to the surrounding deterioration factors. The same CLAP-CRF concentration maintained the previous mortality level, which was credited to the shielding ability exhibited by the CRFs. At day 14, the mortality for CLAP-CRF, 1.2 mg L^{-1}, was still higher than 90%. In contrast, Coragen 1.2 mg L^{-1} decreased to 66.6%.

The biological effectiveness of pesticides gradually decreases with time. As part of the pesticide nanoformulation technology, CLAP-CRF aims to prolong the biological effectiveness half-life as much as possible without creating any hazard stress on the environment. In all treatments, the deterioration in CLAP-CRF

DOI: 10.1021/acs.jafc.7b02560
J. Agric. Food Chem. 2017, 65, 7854−7864

is much lower than that in Coragen, which confirms the thermal and UV shielding ability demonstrated by the CRFs. To configure the CLAP effectiveness life in CLAP-CRF, the 1.2 mg L^{-1} treated trials of CLAP-CRF were kept after day 14 for another 30 days, with samples taken on days 16, 20, 25, 35, and 44. The results showed that CLAP was still effective in realizing 57.66% mortality at day 25, 30.00% mortality at day 35, and 6.66% mortality at day 44.

Conclusion. It has been verified that the attachment of a hydrolyzed α-CD derivative as a gatekeeper on the surface of HMSs offers a suitable method for the design of hollow mesoporous systems that are engineered to deliver entrapped pesticide in the presence of the appropriate enzyme. Specifically, for distinction purposes, the HMS nanoparticles 140, 400, and 1500 nm, under different release stresses (pH and temperature) and permanence under light and thermal stresses, showed different degrees of release behaviors. A clear delivery rate control was additionally found depending on the enzyme used to hydrolyze α-CD derivative. The 400 nm CLAP-CRF release profile in the presence of α-amylase was also examined, whereas the capped CLAP-CRF solids showed "zero release". The same CRFs in water and in the presence of α-amylase released the cargo in a controlled fashion due to the α-1,4 linkages of the anchored α-CD allowing enzyme-induced hydrolysis. The delivery results show that it is possible to design different delivery profiles through a simple selection of the degree of α-CD hydrolysis (i.e., related to the different conditions and their relative properties). The biological activity survey showed that the α-CD functionalized nanoparticles CLAP-CRF are efficiently eaten by *P. xylostella* larvae, although a more effective internalization between *P. xylostella* larvae and CRFs was observed. CLAP-CRF interaction occurs at the chewing step via initiating the saliva production to flow over the eaten leaves' tissues, where the α-CD capping is degraded by the α-amylase enzyme and the cargo is delivered. Finally, the possible application of α-CD functionalized HMSs as suitable delivery systems in preventing insect damage for agrochemical agents such as CLAP was demonstrated, and a substantial reduction of misused pesticides. These results suggest that it might be possible to use gatekeepers as capping systems for the preparation of biocompatible delivery nanodevices for pesticides based on hollow mesoporous silica supports. The opportunity of using these gates that can be selectively unlocked by biomolecules creates a wide range of potential uses in the design of advanced nanodevices for controlled delivery applications pesticides, and several new advances in this area are anticipated. We will also investigate the biological response of the nanoparticles with additional crops and against different insects, including metabolic activities, as well as their ecosystem elimination behavior, which will help us to accumulate information for future field applications.

■ ASSOCIATED CONTENT

Supporting Information

The Supporting Information is available free of charge on the ACS Publications website at DOI: 10.1021/acs.jafc.7b02560.

Synthesis of HMSs, FT-IR spectra, nitrogen absorption-desorption isotherms, and TGA (PDF)

■ AUTHOR INFORMATION

Corresponding Authors

*E-mail: heshun@mail.hzau.edu.cn. Tel: 027-87286968.

*E-mail: jianhl@mail.hzau.edu.cn. Tel: 027-87286968.

ORCID

Amir E. Kaziem: 0000-0002-8125-6889

Shun He: 0000-0003-4551-0744

Funding

This work was supported by the National Natural Science Foundation of China (31601654), Key Projects of Hubei Province Technological Innovation (2016ABA104) and Fundamental Research Funds for the Central Universities (2662015QC011 and 2662016PY109).

Notes

The authors declare no competing financial interest.

■ REFERENCES

(1) Lan, H.; Wang, H.; Chen, Q.; Chen, H.; Jia, D.; Mao, Q.; Wei, T. Small Interfering RNA Pathway Modulates Persistent Infection of a Plant Virus in Its Insect Vector. *Sci. Rep.* **2016**, *6*, 20699.

(2) Allan, G. G.; Chopra, C. S.; Neogi, A. N.; Wilkins, R. M. Design and Synthesis of Controlled Release Pesticide-Polymer Combinations. *Nature* **1971**, *234*, 349−351.

(3) Weissenburger-Moser, L.; Meza, J.; Yu, F.; Shiyanbola, O.; Romberger, D.; LeVan, T. A Principal Factor Analysis to Characterize Agricultural Exposures among Nebraska Veterans. *J. Exposure Sci. Environ. Epidemiol.* **2017**, *27*, 214−220.

(4) Kah, M.; Beulke, S.; Tiede, K.; Hofmann, T. Nanopesticides: State of Knowledge, Environmental Fate, and Exposure Modeling. *Crit. Rev. Environ. Sci. Technol.* **2013**, *43*, 1823−1867.

(5) Khanal, A.; Inoue, Y.; Yada, M.; Nakashima, K. Synthesis of Silica Hollow Nanoparticles Templated by Polymeric Micelle with Core-Shell-Corona Structure. *J. Am. Chem. Soc.* **2007**, *129*, 1534−1535.

(6) Ghosh Chaudhuri, R.; Paria, S. Core/shell Nanoparticles: Classes, Properties, Synthesis Mechanisms, Characterization, and Applications. *Chem. Rev. (Washington, DC, U. S.)* **2012**, *112*, 2373−2433.

(7) Li, Y.; Bastakoti, B. P.; Imura, M.; Tang, J.; Aldalbahi, A.; Torad, N. L.; Yamauchi, Y. Dual Soft-Template System Based on Colloidal Chemistry for the Synthesis of Hollow Mesoporous Silica Nanoparticles. *Chem. - Eur. J.* **2015**, *21*, 6375−6380.

(8) Li, Y.; Bastakoti, B. P.; Yamauchi, Y. Smart Soft-Templating Synthesis of Hollow Mesoporous Bioactive Glass Spheres. *Chem. - Eur. J.* **2015**, *21*, 8038−8042.

(9) Lee, C. H.; Cheng, S. H.; Huang, I. P.; Souris, J.; Yang, C. S.; Mou, C. Y.; Lo, L. W. Intracellular pH-Responsive Mesoporous Silica Nanoparticles for the Controlled Release of Anticancer Chemotherapeutics. *Angew. Chem., Int. Ed.* **2010**, *49*, 8214−8219.

(10) Hao, X.; Hu, X.; Zhang, C.; Chen, S.; Li, Z.; Yang, X.; Liu, H.; Jia, G.; Liu, D.; Ge, K.; Liang, X.; Zhang, J. Hybrid Mesoporous Silica-Based Drug Carrier Nanostructures with Improved Degradability by Hydroxyapatite. *ACS Nano* **2015**, *9*, 9614−9625.

(11) Katagiri, K.; Yamazaki, S.; Inumaru, K.; Koumoto, K. Anti-Reflective Coatings Prepared via Layer-by-Layer Assembly of Mesoporous Silica Nanoparticles and Polyelectrolytes. *Polym. J. (Tokyo, Jpn.)* **2015**, *47*, 190−194.

(12) Leung, K. C.; Chak, C. P. P.; Lo, C. M. M.; Wong, W. Y. Y.; Xuan, S.; Cheng, C. H. pH-Controllable Supramolecular Systems. *Chem. - Asian J.* **2009**, *4*, 364−381.

(13) Yang, Y. W.; Sun, Y. L.; Song, N. Switchable Host−Guest Systems on Surfaces. *Acc. Chem. Res.* **2014**, *47*, 1950−1960.

(14) Saha, S.; Leung, K. C.-F.; Nguyen, T. D.; Stoddart, J. F.; Zink, J. I. Nanovalves. *Adv. Funct. Mater.* **2007**, *17*, 685−693.

(15) Sun, Y.; Ma, J.; Tian, D.; Li, H. Macroscopic Switches Constructed through Host-Guest Chemistry. *Chem. Commun. (Cambridge, U. K.)* **2016**, *52*, 4602−4612.

(16) Nguyen, T.; Leung, K.; Liong, M.; Pentecost, C.; Stoddart, J.; Zink, J. Construction of a pH-Driven Supramolecular Nanovalve. *Org. Lett.* **2006**, *8*, 3363−3366.

(17) Wu, S. H.; Mou, C. Y.; Lin, H. P. Synthesis of Mesoporous Silica Nanoparticles. *Chem. Soc. Rev.* **2013**, *42*, 3862−3875.

(18) Mal, N.; Fujiwara, M.; Tanaka, Y. Photocontrolled Reversible Release of Guest Molecules from Coumarin-Modified Mesoporous Silica. *Nature* **2003**, *421*, 350−353.
(19) Liu, N.; Dunphy, D.; Atanassov, P.; Bunge, S.; Chen, Z.; López, G.; Boyle, T.; Brinker, C. Photoregulation of Mass Transport through a Photoresponsive Azobenzene-Modified Nanoporous Membrane. *Nano Lett.* **2004**, *4*, 551−554.
(20) Aznar, E.; Martínez-Máñez, R.; Sancenón, F. Controlled Release Using Mesoporous Materials Containing Gate-like Scaffoldings. *Expert Opin. Drug Delivery* **2009**, *6*, 643−655.
(21) Cotí, K. K.; Belowich, M. E.; Liong, M.; Ambrogio, M. W.; Lau, Y. A.; Khatib, H. A.; Zink, J. I.; Khashab, N. M.; Stoddart, J. F. Mechanised Nanoparticles for Drug Delivery. *Nanoscale* **2009**, *1*, 16−39.
(22) Nguyen, T.; Liu, Y.; Saha, S.; Leung, K.; Stoddart, J.; Zink, J. Design and Optimization of Molecular Nanovalves Based on Redox-Switchable Bistable Rotaxanes. *J. Am. Chem. Soc.* **2007**, *129*, 626−634.
(23) Liu, R.; Zhao, X.; Wu, T.; Feng, P. Tunable Redox-Responsive Hybrid Nanogated Ensembles. *J. Am. Chem. Soc.* **2008**, *130*, 14418−14419.
(24) Aznar, E.; Marcos, M.; Martínez-Máñez, R.; Sancenón, F.; Soto, J.; Amorós, P.; Guillem, C. pH- and Photo-Switched Release of Guest Molecules from Mesoporous Silica Supports. *J. Am. Chem. Soc.* **2009**, *131*, 6833−6843.
(25) Patel, K.; Angelos, S.; Dichtel, W. R.; Coskun, A.; Yang, Y. W. W.; Zink, J. I.; Stoddart, J. F. Enzyme-Responsive Snap-Top Covered Silica Nanocontainers. *J. Am. Chem. Soc.* **2008**, *130*, 2382−2383.
(26) Bernardos, A.; Aznar, E.; Marcos, M. D.; Martínez-Máñez, R.; Sancenón, F.; Soto, J.; Barat, J.; Amorós, P. Enzyme-Responsive Controlled Release Using Mesoporous Silica Supports Capped with Lactose. *Angew. Chem., Int. Ed.* **2009**, *48*, 5884−5887.
(27) Bernardos, A.; Mondragon, L.; Aznar, E.; Marcos, M. D.; Martinez-Mañez, R.; Sancenon, F.; Soto, J.; Barat, J. M.; Perez-Paya, E.; Guillem, C.; Amorós, P. Enzyme-Responsive Intracellular Controlled Release Using Nanometric Silica Mesoporous Supports Capped with "Saccharides. *ACS Nano* **2010**, *4*, 6353−6368.
(28) Mas, N.; Agostini, A.; Mondragón, L.; Bernardos, A.; Sancenón, F.; Marcos, M. D.; Martínez-Máñez, R.; Costero, A. M.; Gil, S.; Merino-Sanjuán, M.; Amoros, P.; Orzaez, M.; Perezpaya, E. Enzyme-Responsive Silica Mesoporous Supports Capped with Azopyridinium Salts for Controlled Delivery Applications. *Chem. - Eur. J.* **2013**, *19*, 1346−1356.
(29) Leung, K.; Nguyen, T.; Stoddart, F.; Zink, J. Supramolecular Nanovalves Controlled by Proton Abstraction and Competitive Binding. *Chem. Mater.* **2006**, *18*, 5919−5928.
(30) Yang, Q.; Wang, S.; Fan, P.; Wang, L.; Di, Y.; Lin, K.; Xiao, F. S. pH-Responsive Carrier System Based on Carboxylic Acid Modified Mesoporous Silica and Polyelectrolyte for Drug Delivery. *Chem. Mater.* **2005**, *17*, 5999−6003.
(31) Du, L.; Liao, S.; Khatib, H.; Stoddart, F.; Zink, J. Controlled-Access Hollow Mechanized Silica Nanocontainers. *J. Am. Chem. Soc.* **2009**, *131*, 15136−15142.
(32) Khashab, N. M.; Belowich, M. E.; Trabolsi, A.; Friedman, D. C.; Valente, C.; Lau, Y.; Khatib, H. A.; Zink, J. I.; Stoddart, J. F. pH-Responsive Mechanised Nanoparticles Gated by Semirotaxanes. *Chem. Commun. (Cambridge, U. K.)* **2009**, 5371−5373.
(33) Khashab, N.; Trabolsi, A.; Lau, Y.; Ambrogio, M.; Friedman, D.; Khatib, H.; Zink, J.; Stoddart, F. Redox- and pH-Controlled Mechanized Nanoparticles. *Eur. J. Org. Chem.* **2009**, *2009* (11), 1669−1673.
(34) Fu, Q.; Ista, L. K.; Wu, Y.; Andrzejewski, B. P.; Sklar, L. A.; Ward, T. L.; López, G. P.; Rao, G. V. R. Control of Molecular Transport Through Stimuli-Responsive Ordered Mesoporous Materials. *Adv. Mater. (Weinheim, Ger.)* **2003**, *15*, 1262−1266.
(35) Coll, C.; Casasús, R.; Aznar, E.; Marcos, M. D.; Martínez-Máñez, R.; Sancenón, F.; Soto, J.; Amorós, P. Nanoscopic Hybrid Systems with a Polarity-Controlled Gate-like Scaffolding for the Colorimetric Signalling of Long-Chain Carboxylates. *Chem. Commun. (Cambridge, U. K.)* **2007**, *19*, 1957−1959.
(36) Singh, B.; Sharma, D. K.; Gupta, A. A Study towards Release Dynamics of Thiram Fungicide from Starch-Alginate Beads to Control Environmental and Health Hazards. *J. Hazard. Mater.* **2009**, *161*, 208−216.
(37) Ye, Z.; Guo, J.; Wu, D.; Tan, M.; Xiong, X.; Yin, Y.; He, G. Photo-Responsive Shell Cross-Linked Micelles Based on Carboxymethyl Chitosan and Their Application in Controlled Release of Pesticide. *Carbohydr. Polym.* **2015**, *132*, 520−528.
(38) Atta, S.; Paul, A.; Banerjee, R.; Bera, M.; Ikbal, M.; Dhara, D.; Singh, P. Photoresponsive Polymers Based on a Coumarin Moiety for the Controlled Release of Pesticide 2,4-D. *RSC Adv.* **2015**, *5*, 99968−99975.
(39) Sheng, W.; Li, W.; Li, B.; Li, C.; Xu, Y.; Guo, X.; Zhou, F.; Jia, X. Mussel-Inspired Photografting on Colloidal Spheres: A Generalized Self-Template Route to Stimuli-Responsive Hollow Spheres for Controlled Pesticide Release. *Macromol. Rapid Commun.* **2015**, *36*, 1640−1645.
(40) Xu, Y.; Chen, W.; Guo, X.; Tong, Y.; Fan, T.; Gao, H.; Wu, X. Preparation and Characterization of Single- and Double-Shelled Cyhalothrin Microcapsules Based on the Copolymer Matrix of Silica-N-Isopropyl Acrylamide-bis-Acrylamide. *RSC Adv.* **2015**, *5*, 52866−52873.
(41) Sheng, W.; Li, W.; Zhang, G.; Tong, Y.; Liu, Z.; Jia, X. Study on the UV-Shielding and Controlled-Release Properties of a Polydopamine Coating for Avermectin. *New J. Chem.* **2015**, *39*, 2752−2757.
(42) Yi, Y.; Xu, S.; Sun, H.; Chang, D.; Yin, Y.; Zheng, H.; Xu, H.; Lou, Y. Gelation of Photocrosslinkable Carboxymethyl Chitosan and Its Application in Controlled Release of Pesticide. *Carbohydr. Polym.* **2011**, *86*, 1007−1013.
(43) Liu, B.; Wang, Y.; Yang, F.; Wang, X.; Shen, H.; Cui, H.; Wu, D. Construction of a Controlled-Release Delivery System for Pesticides Using Biodegradable PLA-Based Microcapsules. *Colloids Surf., B* **2016**, *144*, 38−45.
(44) Campos, E. V. V; De Oliveira, J. L.; Da Silva, C. M.; Pascoli, M.; Pasquoto, T.; Lima, R.; Abhilash, P. C.; Fraceto, L. F. Polymeric and Solid Lipid Nanoparticles for Sustained Release of Carbendazim and Tebuconazole in Agricultural Applications. *Sci. Rep.* **2015**, *5* (5), 13809−13823.
(45) Frederiksen, H. K.; Kristensen, H. G.; Pedersen, M. Solid Lipid Microparticle Formulations of the Pyrethroid Gamma-Cyhalothrin-Incompatibility of the Lipid and the Pyrethroid and Biological Properties of the Formulations. *J. Controlled Release* **2003**, *86*, 243−252.
(46) Ruiz-Hitzky, E.; Aranda, P.; Darder, M.; Rytwo, G. Hybrid Materials Based on Clays for Environmental and Biomedical Applications. *J. Mater. Chem.* **2010**, *20*, 9306−9321.
(47) Kovacević, D.; Lemić, J.; Damjanović, M.; Petronijević, R. Janaćković, Đ.; Stanić, T. Fenitrothion Adsorption-Desorption on Organo-Minerals. *Appl. Clay Sci.* **2011**, *52*, 109−114.
(48) Bakhtiary, S.; Shirvani, M.; Shariatmadari, H. Adsorption-Desorption Behavior of 2,4-D on NCP-Modified Bentonite and Zeolite: Implications for Slow-Release Herbicide Formulations. *Chemosphere* **2013**, *90*, 699−705.
(49) Shirvani, M.; Farajollahi, E.; Bakhtiari, S.; Ogunseitan, O. Mobility and Efficacy of 2,4-D Herbicide from Slow-Release Delivery Systems Based on Organo-Zeolite and Organo-Bentonite Complexes. *J. Environ. Sci. Health, Part B* **2014**, *49*, 255−262.
(50) Liu, W.; Yao, J.; Cai, M.; Chai, H.; Zhang, C.; Sun, J.; Chandankere, R.; Masakorala, K. Synthesis of a Novel Nanopesticide and Its Potential Toxic Effect on Soil Microbial Activity. *J. Nanopart. Res.* **2014**, *16*, 1−13.
(51) Sarlak, N.; Taherifar, A.; Salehi, F. Synthesis of Nanopesticides by Encapsulating Pesticide Nanoparticles Using Functionalized Carbon Nanotubes and Application of New Nanocomposite for Plant Disease Treatment. *J. Agric. Food Chem.* **2014**, *62*, 4833−4838.
(52) Aznar, E.; Villalonga, R.; Giménez, C.; Sancenón, F.; Marcos, D.; Martínez-Máñez, R.; Díez, P.; Pingarrón, J.; Amorós, P. Glucose-Triggered Release Using Enzyme-Gated Mesoporous Silica Nanoparticles. *Chem. Commun.* **2013**, *49*, 6391−6393.
(53) Guo, M.; Zhang, W.; Ding, G.; Guo, D.; Zhu, J.; Wang, B.; Punyapitak, D.; Cao, Y. Preparation and Characterization of Enzyme-Responsive Emamectin Benzoate Microcapsules Based on a Copolymer

DOI: 10.1021/acs.jafc.7b02560
J. Agric. Food Chem. 2017, 65, 7854−7864

Matrix of Silica−Epichlorohydrin-Carboxymethylcellulose. *RSC Adv.* **2015**, *5*, 93170−93179.
(54) Li, Z. Z.; Xu, S. A.; Wen, L. X.; Liu, F.; Liu, A. Q.; Wang, Q.; Sun, H. Y.; Yu, W.; Chen, J. F. Controlled Release of Avermectin from Porous Hollow Silica Nanoparticles: Influence of Shell Thickness on Loading Efficiency, UV-Shielding Property and Release. *J. Controlled Release* **2006**, *111*, 81−88.
(55) Sharma, S. K.; Zimmerman, W. T.; Singles, S. K.; Malekani, K.; Swain, S.; Ryan, D.; Mcquorcodale, G.; Wardrope, L. Photolysis of Chlorantraniliprole and Cyantraniliprole in Water and Soil: Verification of Degradation Pathways via Kinetics Modeling. *J. Agric. Food Chem.* **2014**, *62*, 6577−6584.
(56) Jiang, X.; Luo, L.; Zhang, L.; Sappington, T.; Hu, Y. Regulation of Migration in *Mythimna separata* (Walker) in China: A Review Integrating Environmental, Physiological, Hormonal, Genetic, and Molecular Factors. *Environ. Entomol.* **2011**, *40*, 516−533.
(57) Xu, W.; Huang, Q.; Wu, X.; Yu, X.; Wang, X.; Tao, L. Property of Midgut α-Amylase From *Mythimna separata* (Lepidoptera: Noctuidae) Larvae and Its Responses to Potential Inhibitors In Vitro. *J. Insect Sci.* **2014**, *14*, 282−282.
(58) Qi, G.; Wang, Y.; Estevez, L.; Switzer, A.; Duan, X.; Yang, X.; Giannelis, E. Facile and Scalable Synthesis of Monodispersed Spherical Capsules with a Mesoporous Shell. *Chem. Mater.* **2010**, *22*, 2693−2695.
(59) Del Valle, E. M. M. Cyclodextrins and Their Uses: a Review. *Process Biochem.* **2004**, *39*, 1033−1046.

DOI: 10.1021/acs.jafc.7b02560
J. Agric. Food Chem. 2017, 65, 7854−7864